

# Quantum Resonant Dimensionality Reduction and Its Application in Quantum Machine Learning

Fan Yang,<sup>1,2,\*</sup> Furong Wang,<sup>3,\*</sup> Xusheng Xu,<sup>2</sup> Pao Gao,<sup>1</sup> Tao Xin,<sup>4</sup> ShiJie Wei,<sup>1,†</sup> and Guilu Long<sup>2,5,6,‡</sup>

<sup>1</sup>*Beijing Academy of Quantum Information Sciences, Beijing 100193, China*

<sup>2</sup>*State Key Laboratory of Low-Dimensional Quantum Physics and  
Department of Physics, Tsinghua University, Beijing 100084, China*

<sup>3</sup>*China North Vehicle Research Institute, Beijing 100072, China*

<sup>4</sup>*Shenzhen Institute for Quantum Science and Engineering,  
Southern University of Science and Technology, Shenzhen 518055, China*

<sup>5</sup>*Tsinghua National Laboratory for Information Science and Technology, Beijing 100084, People's Republic of China*

<sup>6</sup>*Collaborative Innovation Center of Quantum Matter, Beijing 100084, China*

Quantum computing is a promising candidate for accelerating machine learning tasks. Limited by the control accuracy of current quantum hardware, reducing the consumption of quantum resources is the key to achieving quantum advantage. Here, we propose a quantum resonant dimension reduction (QRDR) algorithm based on the quantum resonant transition to reduce the dimension of input data and accelerate the quantum machine learning algorithms. After QRDR, the dimension of input data  $N$  can be reduced into desired scale  $R$ , and the effective information of the original data will be preserved correspondingly, which will reduce the computational complexity of subsequent quantum machine learning algorithms or quantum storage. QRDR operates with polylogarithmic time complexity and reduces the error dependency from the order of  $1/\epsilon^3$  to the order of  $1/\epsilon$ , compared to existing algorithms. We demonstrate the performance of our algorithm combining with two types of quantum classifiers, quantum support vector machines and quantum convolutional neural networks, for classifying underwater detection targets and quantum many-body phase respectively. The simulation results indicate that reduced data improved the processing efficiency and accuracy following the application of QRDR. As quantum machine learning continues to advance, our algorithm has the potential to be utilized in a variety of computing fields.

## I. INTRODUCTION

Machine learning has proven to be a remarkably powerful tool with broad practical applications across various fields of science and engineering, including finance [1, 2], medical science [3, 4], and the simulation of classical and complex quantum systems. It has shown notable success in compressing high-dimensional data, where near-term quantum devices may offer significant speed enhancements [5]. Given the potential quantum advantage of quantum computing, numerous quantum machine learning (QML) algorithms have been proposed [6], such as quantum recommendation systems (QRS) [7], quantum support vector machines (QSVM) [8], quantum principal component analysis (QPCA) [9], and quantum neural networks [10, 11], among others.

In machine learning, dimensionality reduction (DR) is a valuable technique for refining information and significantly decreasing data processing time. DR involves compressing high-dimensional datasets into lower-dimensional representations while preserving key information from the original dataset. Principle component analysis (PCA) DR is the most representative example of linear DR. It works by projecting the original data onto the subspace of the covariance matrix with larger singular

values while disregarding components with smaller values. These smaller principal components often represent noise, so dimensionality reduction can enhance the accuracy of subsequent data processing. By applying kernel methods, kernel principal component analysis (KPCA) extends the concept of PCA to enable nonlinear dimensionality reduction.

In recent years, several quantum dimensionality reduction (QDR) methods have been proposed. Here we focus on an important type, the PCA-based QDR algorithms, which can efficiently remove redundant information by identifying orthogonal principal components, reducing computational complexity, and enhancing model performance, especially in high-dimensional datasets. Among PCA-based QDR algorithms, the most renowned one is quantum principal component analysis (QPCA) [9], which uses density matrices to obtain their eigenvalues and eigenstates. In QPCA, quantum amplitude estimation and quantum phase estimation (QPE) are also necessary for preparing data vectors after DR, but they demand significant quantum resources. Following QPCA, two approaches can achieve QDR, one is QPE-based QDR [12, 13] and the other is variational quantum algorithm (VQA)-based QDR [14]. QPE-based algorithms have reduced time complexity compared to QPCA. They still face challenges related to the required number of ancilla qubits and evolution time, posing difficulties for current state-of-the-art quantum computers. In contrast, VQA-based algorithms are generally seen as friendly for noisy intermediate-scale quantum (NISQ) devices, but its

\* These authors contributed equally to this work.

† [weisj@baqis.ac.cn](mailto:weisj@baqis.ac.cn)

‡ [gllong@tsinghua.edu.cn](mailto:gllong@tsinghua.edu.cn)

complexity becomes increasingly challenging to analyze as the number of qubits grows.

There are also many other types of quantum dimension reduction algorithms, like based on autoencoders [15, 16], A-optimal projection [17, 18], linear discriminant analysis [19, 20] and locally linear embedding [21, 22]. These algorithms are based on different data mining principles and are used in different data sets and different demand scenarios. We don't go to details here.

To address these challenges, we introduce a novel quantum dimensionality reduction algorithm called quantum resonant dimensionality reduction (QRDR), based on quantum resonant transitions (QRT) [23, 24]. By employing QRT instead of QPE, the number of ancilla qubits is reduced from  $O(1/\epsilon + \log R)$  to  $O(\log R)$  in QRDR that is independent of the accuracy  $\epsilon$ , offering an advantage over other quantum DR algorithms such as QPE-based methods [12, 13]. In contrast to VQA-DR, our QRDR presents an exact time complexity. Compared to QPE-based DR algorithm and QPCA algorithm, the time complexity of QRDR is reduced from the order  $1/\epsilon^3$  to the order  $1/\epsilon$ . We simulate the QRDR algorithm numerically and evaluate its performance using quantum support vector machines and quantum convolutional neural networks (QCNN). The results demonstrate that our QRDR effectively reduces the dimension of quantum data, enabling various quantum machine learning algorithms to process the data more efficiently post-reduction.

The remainder of this paper is organized as follows: Sec. II provides the framework of the algorithm and details the quantum resources consumed. Sec. III presents the simulation results of applying QRDR in quantum support vector machines and quantum convolutional neural networks. In Sec. IV, we compare our algorithm with existing approaches and conclude with a summary of our findings.

## II. THE FRAMEWORK OF THE ALGORITHM

### A. Principal component analysis dimension reduction and its quantum expression

Principal component analysis for dimensionality reduction relies on linear transformations involving the covariance matrix (or kernel matrix). In this paper, we focus on the basic PCA method, leaving out advanced techniques such as kernel methods and centering, which are detailed in references [12, 13].

The original data before DR can be represented as a matrix  $X \in \mathbb{R}^{M \times N}$ , where the  $i$ th row of  $X$  corresponds to the  $i$ th sample,  $\mathbf{x}_i = [x_i^1, x_i^2, \dots, x_i^N]$ , containing  $N$  features. The covariance matrix of this data, denoted as  $A \in \mathbb{R}^{N \times N} = X^T X$ . The data undergoes singular value

decomposition (SVD) as follows

$$X = \sum_{k=1}^M \sigma_k \mathbf{u}_k^T \mathbf{v}_k, \quad (1)$$

where  $\mathbf{u}_k$  and  $\mathbf{v}_k$  are singular vectors corresponding to singular value  $\sigma_k$ . It is usually assumed that the singular values are ordered from largest to smallest. The matrix  $A$  has eigenvalue decomposition

$$A = \sum_{k=1}^M \sigma_k^2 \mathbf{v}_k^T \mathbf{v}_k. \quad (2)$$

By definition,  $A$  is the Hermitian matrix and the  $k$ -th eigenvalue is  $\lambda_k = \sigma_k^2$  with eigenvector  $\mathbf{v}_k$ . When the dimension is reduced from  $N$  to  $R$ , the data matrix  $Z \in \mathbb{R}^{M \times R}$  after dimensionality reduction can be represented by the formula  $Z = X V_R^T$ . The matrix  $V_R$  is a projection matrix composed of the first  $R$  singular vectors, with each row  $j$  of  $V_R$  corresponding to the  $j$ th singular vector  $\mathbf{v}_j$ . Consequently, the value of the  $j$ -th feature for  $z_i$  is given by  $z_i^j = \mathbf{x}_i \cdot \mathbf{v}_j^T$ .

For the QDR, the input is a quantum state that encodes the information from the original data

$$|X\rangle = \sum_{i=1}^M \sum_{j=1}^N x_i^j |j\rangle |i\rangle = \sum_{i=1}^M \|x_i\| |x_i\rangle |i\rangle, \quad (3)$$

where  $|i\rangle$  and  $|j\rangle$  represent quantum computational basis states, and  $|x_i\rangle = \frac{1}{\|x_i\|} \sum_{j=1}^N x_i^j |j\rangle$  with the normalized coefficient  $\|x_i\| = \sqrt{\sum_{j=1}^N |x_i^j|^2}$ . The output state of QDR is given by

$$|Z\rangle = \sum_{i=1}^M \sum_{j=1}^R z_i^j |j\rangle |i\rangle = \sum_{i=1}^M \|z_i\| |z_i\rangle |i\rangle. \quad (4)$$

The goal of QDR is to prepare the state  $|Z\rangle$  as described in Eq.(4). In this section, the overall normalization coefficients for the quantum states are omitted.

### B. Quantum Resonant Dimensionality Reduction Algorithm

We use quantum resonant transitions (QRT) to realize the dimensionality reduction process, which includes designing the Hamiltonian and implementing the time evolution operator. Here we take one of the  $M$  samples,  $N$  dimensional vector  $\mathbf{x}$ , as the original data. Our algorithm utilizes one probe qubit to find the eigenstate,  $n = \lceil \log_2 N \rceil$  qubits to store the state corresponding to the original data, and  $r = \lceil \log_2 R \rceil$  qubits to store the state after dimensionality reduction. The Hamiltonian is defined as follows

$$\mathcal{H} = |0\rangle\langle 0| \otimes (|0\rangle\langle 0|^{\otimes r} - I_2^{\otimes r}) \otimes I_2^{\otimes n} + |1\rangle\langle 1| \otimes H_p + \frac{c\pi}{2} \sigma_y \otimes B \otimes I_2^{\otimes n}. \quad (5)$$

Here  $c$  represents the resonant parameter,  $\sigma_y$  is the Pauli matrix, and  $B = \sqrt{2^r} H_d^{\otimes r}$ , where  $H_d = \frac{1}{\sqrt{2}}[1, 1; 1, -1]$  is the Hadamard matrix. The three terms in Equation (5) correspond to the Hamiltonian of the probe qubit, the problem Hamiltonian, and their interaction, respectively. Specifically, the second term,  $H_p$ , can be expressed as follows

$$H_p = H_\lambda \otimes I_2^{\otimes n} + I_2^{\otimes r} \otimes A, \quad (6)$$

where  $H_\lambda$  is a diagonal matrix that encodes the  $R$  eigenvalues  $\lambda_k = \sigma_k^2$  of the covariance matrix  $A$ . The diagonal elements of  $H_\lambda$  are given by  $h_k = -\lambda_k$ . Given the original data  $\mathbf{x}$ , the input state  $|\psi\rangle_{in}$  is represented as  $|0\rangle|0\rangle^{\otimes r}|x\rangle$ . This typically requires specialized quantum devices such as quantum random access memory (QRAM) [25] to implement. The state can also be expanded in terms of the eigenvectors of  $A$  as

$$|\psi\rangle_{in} = |0\rangle|0\rangle|x\rangle = |0\rangle|0\rangle^{\otimes r} \sum_{k=1}^N z^k |v_k\rangle, \quad (7)$$

where  $z^k = \langle v_k | x \rangle$ . Setting  $t = 1/c$ , the state after the application of the Hamiltonian evolution operator  $e^{-i\mathcal{H}t}$  is

$$\begin{aligned} e^{-i\mathcal{H}t} |\psi\rangle_{in} &= |1\rangle \sum_{k=1}^R z^k |k\rangle |v_k\rangle \\ &+ |0\rangle \sum_{k'=R+1}^N |0\rangle^{\otimes r} z^{k'} |v_{k'}\rangle. \end{aligned} \quad (8)$$

It is assumed that  $c$  is much smaller than the minimum difference between eigenvalues of  $H$ , allowing us to neglect the effects of off-resonance. A detailed analysis of the dynamics, errors, and time complexity will be provided in the next section.

To obtain the low-dimensional state, the probe qubit must be collapsed to state  $|1\rangle$  and the second and third registers disentangled. It means that we need to perform additional operations to make the quantum state evolve from  $|k\rangle|v_k\rangle$  to  $|k\rangle|0\rangle$ , for each  $k$ . We employ the method proposed in Ref. [13], which utilizes a reference state  $|\psi\rangle$  and its corresponding inverse unitary operator  $U_\psi^{-1}|\psi\rangle = |0\rangle^{\otimes n}$  to achieve this step. The projection  $\phi_k$  of the reference state and each eigenstate  $v_k$  needs to be measured. Then, apply the inverse unitary operator and controlled rotations to the ancilla qubits and work qubits for different wave vectors  $k$ . The final state is obtained in the second register is

$$|\psi\rangle_{out} = |1\rangle \sum_{k=1}^R z^k |k\rangle |0\rangle^{\otimes n}. \quad (9)$$

According to the above derivation, we take  $|X\rangle$  that defined in Eq. 3 as original data state, the input state can be expressed as

$$|\Psi\rangle_{in} = |0\rangle|0\rangle^{\otimes r}|X\rangle = |0\rangle|0\rangle^{\otimes r} \sum_{i=1}^M \|x_i\| |x_i\rangle |i\rangle. \quad (10)$$

The evolution operator does not affect the serial number state  $|i\rangle$ , so the state after applying the operator is

$$|1\rangle \sum_{i=1}^M \sum_{k=1}^R z_i^k |k\rangle |v_k\rangle |i\rangle + |0\rangle|0\rangle^{\otimes r} \sum_{i=1}^M \sum_{k'=R+1}^N z_i^{k'} |v_{k'}\rangle |i\rangle, \quad (11)$$

where  $z_i^k = \langle v_k | x_i \rangle$ . After measuring the probe qubit and disentangling the second and third registers, the final state is consistent with Eq. (4)

$$|\Psi\rangle_{out} = |1\rangle \sum_{i=1}^M \|z_i\| |z_i\rangle |i\rangle |0\rangle^{\otimes n} = |1\rangle |Z\rangle |0\rangle^{\otimes n}, \quad (12)$$

which is the output state of the algorithm. The QRDR process can be summarized in Alg.1 The different pro-

---

### Algorithm 1: Quantum Resonant Dimensionality Reduction

---

**Inputs:** Dataset state  $|X\rangle$ , covariance matrix  $A$  and its first  $R$  eigenvalues  $\lambda_k, k \in [1, R]$ .

*step 1:* Prepare the initial state  $|0\rangle|0\rangle^{\otimes r}|X\rangle$ .

*step 2:* Set appropriate resonant parameter  $c$ .

*step 3:* Simulate the Hamiltonian  $\mathcal{H}$  for a duration time of  $t = 1/c$ .

*step 4:* Measure the probe qubit and proceed if the measurement result is  $|1\rangle$ .

*step 5:* Disentangle the second and third registers using  $U_\psi^{-1}|\psi\rangle$ .

**Outputs:**  $|1\rangle|Z\rangle|0\rangle^{\otimes n}$ .

---

cedures for dimension reduction using QRDR, QPE-DR, and QPCA are shown in Fig.[? ].

### C. Errors and Complexity of QRDR

In this section, we give the details of the key step of QRDR, implementing time evolution operator  $e^{-i\mathcal{H}t}$  [12, 13]. We provide the specific procedures that how does the quantum state evolve from Eq. (7) to Eq. (8). Assuming the input state is the eigenstate of matrix  $A$

$$|\Psi\rangle_{in} = |0\rangle|0\rangle^{\otimes r}|v_k\rangle, \quad (13)$$

where  $k \leq R$ . Without considering interaction term  $\frac{c\pi}{2}\sigma_y \otimes B \otimes I_2^{\otimes n}$ , the other parts of Hamiltonian are

$$\mathcal{H}' = |0\rangle\langle 0| \otimes (|0\rangle\langle 0|^{\otimes r} - I_2^{\otimes r}) \otimes I_2^{\otimes n} + |1\rangle\langle 1| \otimes H_p. \quad (14)$$

$|\Psi\rangle_{in}$  is the eigenstate of  $\mathcal{H}'$  with eigenvalue 0. For the second part of  $\mathcal{H}'$ ,  $|1\rangle|j\rangle|v_k\rangle$  are also the eigenstates with eigenvalues  $\lambda_k - \lambda_j$ . If  $j = k$ , it has eigenvalues  $\lambda_k - \lambda_j = 0$ , which are same with  $|0\rangle|0\rangle^{\otimes r}|v_k\rangle$ .

Firstly, we consider the dynamics between  $|0\rangle|0\rangle^{\otimes r}|v_k\rangle$  and  $|1\rangle|j\rangle|v_j\rangle$  ( $j, k \leq R$ ) because of their same eigenvalues 0. For each pair of  $|0\rangle|0\rangle^{\otimes r}|v_k\rangle$  and  $|1\rangle|j\rangle|v_j\rangle$ ,  $\mathcal{H}$  in this subspace can be written as [26]

$$\mathcal{H}_{kj} = \begin{bmatrix} 0 & -id_{kj} \\ id_{kj}^* & 0 \end{bmatrix}, \quad (15)$$

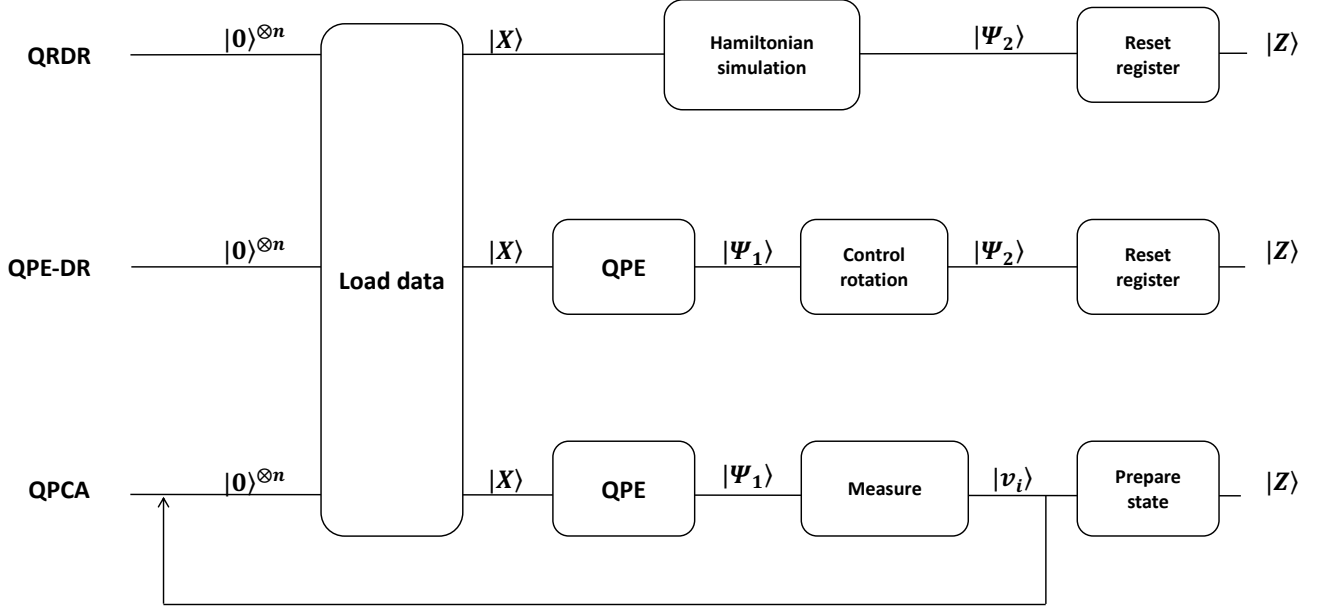


FIG. 1. The procedures for dimension reduction using QRDR, QPE-DR, and QPCA differ significantly. The main distinction between QRDR and QPE-DR lies in the use of the Hamiltonian, which replaces the need for QPE and controlled rotation operators in QRDR. In contrast, QPCA requires the use of QPE and involves repeated measurements of auxiliary qubits.

where  $d_{kj} = \frac{c\pi}{2} \langle 0|^{\otimes r} B |j\rangle \langle v_k | I_2^{\otimes n} |v_j\rangle = \frac{1}{2} c\pi \delta_{kj}$ .  $\delta_{kj}$  is 1 if and only if  $j = k$ , and 0 otherwise. It means that resonant transitions just happens between  $|0\rangle|0\rangle^{\otimes r}|v_k\rangle$  and  $|1\rangle|k\rangle|v_k\rangle$ . So the state in Eq. (13) after evolution operator  $e^{-i\mathcal{H}t}$  is

$$e^{-i\mathcal{H}t} |\Psi_{in}\rangle = \cos\left(\frac{c\pi t}{2}\right) |0\rangle|0\rangle^{\otimes r}|v_k\rangle + \sin\left(\frac{c\pi t}{2}\right) |1\rangle|k\rangle|v_k\rangle. \quad (16)$$

In setting  $t = 1/c$ , the state is  $|1\rangle|k\rangle|v_k\rangle$  after this step.

The other case is off-resonance that happens between  $|0\rangle|0\rangle^{\otimes r}|v_k\rangle$  and  $|1\rangle|j\rangle|v_{k'}\rangle$ . Here  $j \neq k'$ , and in this subspace  $\mathcal{H}$  is a little different with Eq. (15)

$$\mathcal{H}_{kj k'} = \begin{bmatrix} 0 & -id_{kj k'} \\ id_{kj k'}^* & \lambda_{k'} - \lambda_j \end{bmatrix}. \quad (17)$$

Here  $d_{kj k'} = \frac{1}{2} c\pi \delta_{kk'}$ , so the resonant transition just happens when  $k = k'$  and the amplitude of this small off-resonance is

$$\begin{aligned} b_{kj k'} &= \frac{c\pi |d_{kj k'}|}{\sqrt{(c\pi |d_{kj k'}|)^2 + |\lambda_{k'} - \lambda_j|^2}} \\ &= \frac{c\pi \delta_{kk'}}{\sqrt{(c\pi \delta_{kk'})^2 + |\Delta_{jk'}|^2}} \\ &\leq \frac{c\pi \delta_{kk'}}{|\Delta_{jk'}|} = \mathcal{O}(c/\Delta_{min}), \end{aligned} \quad (18)$$

where  $\Delta_{min}$  denotes the min energy gap  $\Delta_{min} = \min |E_{i+1} - E_i|$ . For the other eigenstates that  $k > R$ , they always fit  $k \neq j$  and almost stay in original state with a small off-resonance.

Therefore, considering the off-resonance error, the input state in Eq. (7) after evolution operator  $e^{-i\mathcal{H}/c}$  is

$$\begin{aligned} |1\rangle \sum_{k=1}^R z^k \alpha_k |k\rangle |v_k\rangle + \sum_{k'=R+1}^N |0\rangle|0\rangle^{\otimes r} z^{k'} \alpha'_k |v_{k'}\rangle \\ + \mathcal{O}(c/\Delta_{min}) |\Psi\rangle_e. \end{aligned} \quad (19)$$

$|\Psi\rangle_e$  is the error state here, and  $\alpha_k \geq \sqrt{1 - \sum_{j \neq k} b_{kj k}^2}$ . Because the sum of  $1/n^2$  sequences is converged, it has

$$\begin{aligned} |\alpha_k|^2 &\geq 1 - \sum_{j \neq k} |b_{kj k}|^2 \\ &\geq 1 - (c\pi)^2 \sum_{j \neq k} 1/|\Delta_{jk}|^2 \\ &\geq 1 - \left(\frac{c\pi}{\Delta_{min}}\right)^2 \sum_{j \neq k} 1/|j - k|^2 \\ &= 1 - \mathcal{O}(c^2/\Delta_{min}^2). \end{aligned} \quad (20)$$

Defining the fidelity as

$$\epsilon = 1 - |\langle Z | \Psi \rangle_{out}|^2 = \mathcal{O}(c^2/\Delta_{min}^2), \quad (21)$$

so that the query complexity for time evolution step is

$$\begin{aligned} \mathcal{O}(d \|\mathcal{H}\|_{max} \text{polylog}(MN)t) &= \\ \mathcal{O}(d \|A\|_{max} \text{polylog}(MN)/c) &= \\ \mathcal{O}(d \|A\|_{max} \text{polylog}(MN)/\Delta_{min} \epsilon^{0.5}). \end{aligned} \quad (22)$$

Here  $d$  is the sparsity of  $A$ .

QRDR's time complexity mainly consists of three parts: obtaining eigenvalues, Hamiltonian evolution, and

decoupling. Firstly, QRDR requires the eigenvalues of matrix  $A$ . In previous work [27], it has been proved that the error  $\epsilon$  is proportional to accuracy of eigenvalues, so the complexity of obtaining the first  $R$  eigenvalues is  $\mathcal{O}(Rd\|A\|_{\max}\text{polylog}(MN)/\epsilon)$ . For the initial state, it can be prepared in time  $\mathcal{O}(\text{polylog}(MN))$  according to the QRAM [25]. In *step 4*, the probability of success is constant if the first  $R$  eigenvalues are enough to reconstruct  $A$  as  $\sum_{k=1}^R \sigma_k^2 \approx \sum_{k'=1}^N \sigma_{k'}^2$ . Secondly, the query complexity for Hamiltonian evolution is  $\mathcal{O}(d\|A\|_{\max}\text{polylog}(MN)/\Delta_{\min}\epsilon^{0.5})$ . Finally, the query complexity of decoupling corresponding to *step 5* is  $\mathcal{O}(R^{1.5}d\|A\|_{\max}\text{polylog}(MN)/\epsilon)$  [13]. We use the method in Ref.[28] to achieve the Hamiltonian time evolution operator, and other approaches like VQAs-based methods [29–31] are also applicable.

In conclusion, the total time complexity of QRDR is

$$\begin{aligned} &\mathcal{O}(Rd\|A\|_{\max}\text{polylog}(MN)/\epsilon + \\ &d\|A\|_{\max}\text{polylog}(MN)/\Delta_{\min}\epsilon^{0.5} + \\ &R^{1.5}d\|A\|_{\max}\text{polylog}(MN)/\epsilon). \end{aligned} \quad (23)$$

Under the condition that  $R = \mathcal{O}(\text{polylog}N)$  eigenvalues can reconstruct the covariance matrix  $A$ , and  $\Delta_{\min} = \mathcal{O}(\epsilon^{0.5}/R)$ , the time complexity is simplified to  $\mathcal{O}(d, \text{polylog}(MN)/\epsilon)$ . The following discussion of QPE-based QDR and QPCA assumes the same conditions, where  $R = \mathcal{O}(\text{polylog}N)$ . QPE-based QDR [12, 13] solve the PCADR problem using quantum phase estimation, which can prepare the eigenvalues in ancilla qubits. As shown in Fig. 1, it applies QPE to data state  $|x\rangle$  and obtained the state

$$|\Psi_1\rangle = \Psi \sum_{i=1}^M \sum_{j=0}^N z_i^j |\hat{\sigma}_j\rangle |v_j\rangle |i\rangle. \quad (24)$$

Then it uses control rotation operator like HHL method to remove the eigenstate corresponding to the eigenvalue after the  $R$ -th eigenvalue and applies the inverse operation of QPE, then the state is

$$|\Psi_2\rangle = \sum_{i=1}^M \sum_{j=1}^R z_i^j |v_j\rangle |i\rangle. \quad (25)$$

$|v_i\rangle$  is the  $i$ -th eigenstate of  $XX^\dagger$ . QRDR can achieve the same steps by simulating the Hamiltonian in Eq. 5. The runtime of this QPE-based DR algorithm is  $\mathcal{O}(d, \text{polylog}(MN)/\epsilon^3)$ . The complexity of QRDR is  $\mathcal{O}(d, \text{polylog}(MN)/\epsilon)$  under the assumption that  $\|A\|_{\max}$  is  $\mathcal{O}(1)$  order. In the circumstances  $\Delta_{\min} = \mathcal{O}(\epsilon^{0.5}/R)$ , our algorithm provides the advantage of polynomial order in accuracy  $\epsilon$  compared to QPE-based QDR. Additionally, QPE requires an extra  $\mathcal{O}(1/\epsilon)$  qubits to recover the eigenvalues, whereas QRDR does not require this extra quantum register. QPCA [9] and Resonant QPCA [24] can reduce the dimension of the quantum state, but they must solve each of the  $R$  eigenvalues and  $M$  samples one by one, as shown in Fig. 1, resulting in a complexity of  $\mathcal{O}(MR)$ . Detailed results are shown in the Table I.

### III. NUMERICAL SIMULATION RESULTS OF QRDR IN QUANTUM MACHINE LEARNING

In this section, we use the QRDR method to reduce the dimensionality of data prior to its use in quantum machine learning algorithms. First, we assess the precision of our quantum algorithm by comparing the results of quantum dimensionality reduction with theoretical expectations. We then apply two distinct quantum classification algorithms to measure the efficiency of QRDR.

There are two primary reasons for choosing classification as the subsequent task: First, classification tasks allow for easy evaluation of data quality. If the data resulting from QRDR cannot be effectively classified (e.g., through a decrease in final accuracy), it indicates that some useful information may have been lost during the process. Second, accuracy can be used to gauge the convergence rate of quantum machine learning algorithms, which are two key performance indicators for many machine learning tasks. The numerical simulation process is summarized in Fig. 2.

#### A. QRDR FOR QUANTUM SUPPORT VECTORS MACHINE

In this section, *Connectionist Bench (Sonar, Mines vs. Rocks) Data Set* is used to evaluate our QRDR algorithm. This dataset includes samples of mines and rocks. First, we apply QRDR to reduce the dimensionality of the dataset. Then, we use a quantum support vector machine (QSVM) to classify the data before and after QRDR. The algorithm simulation flow in this section is consistent with that in Fig. 2, with taking QSVM as the quantum classifier. The main steps of QRDR were discussed in the previous section, while the steps of QSVM are briefly outlined here.

The input of the quantum support vector machine (QSVM) is a data matrix  $A \in \mathbb{R}^{M \times N}$ , containing  $M$  distinct sample vectors  $\mathbf{x}_i$ , each with  $N$  parameters. Each  $i$ -th sample is assigned a label  $y_i$  to classify this sample. The objective of QSVM is to train a quantum state in  $N + 1$  dimensions, enabling the classification of new vectors  $\mathbf{x}'$  by determining their label  $y'$ .

The core step of QSVM is to solve the following linear equation using a quantum computer

$$\begin{pmatrix} \eta_0 \\ \boldsymbol{\eta} \end{pmatrix} = A^{-1} \begin{pmatrix} 0 \\ \mathbf{y} \end{pmatrix}, A = \begin{pmatrix} 0 & \vec{\mathbf{1}}^T \\ \vec{\mathbf{1}} & \mathcal{K} + \gamma^{-1}I \end{pmatrix}. \quad (26)$$

$\mathcal{K}$  is the kernel matrix with the element  $\mathcal{K}_{jk} = \mathbf{x}_j^T \cdot \mathbf{x}_k$ .  $\mathbf{y} = (y_1, \dots, y_M)^T$  and  $\vec{\mathbf{1}} = (1, \dots, 1)^T$ . The hyperplane can be constructed by  $\mathbf{w} = \sum_{j=1}^M \eta_j \mathbf{x}_j$  and  $w_0 = \eta_0$ . There are several quantum algorithms available for solving this problem, such as the HHL method [32], variational quantum linear solvers, and others [33, 34]. Once the state  $|\eta_0, \boldsymbol{\eta}\rangle$  has been prepared, the label of a new

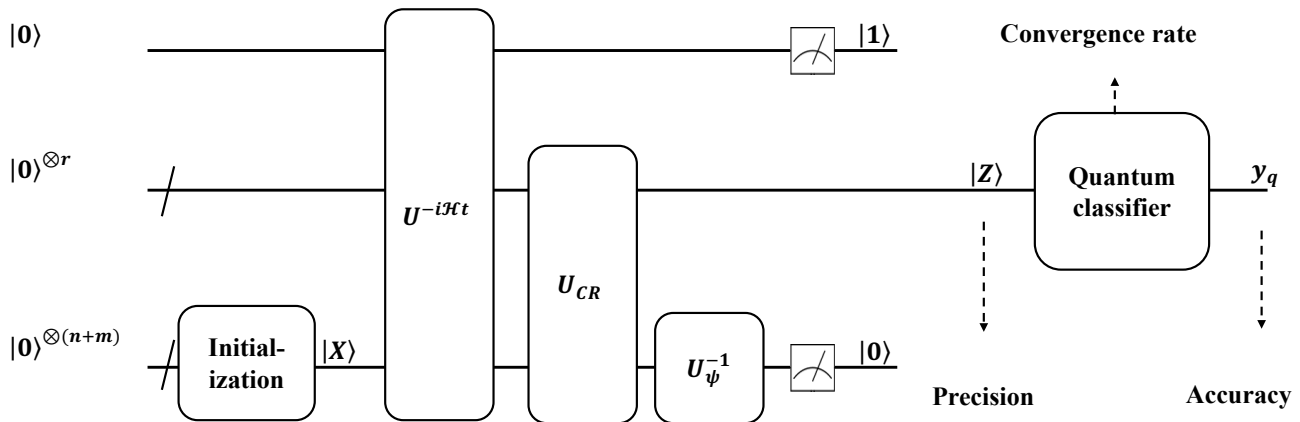


FIG. 2. The Schematic quantum circuits of simulating QRDR in quantum machine learning. The two blue parts are the simulated result of quantum algorithms in the classical computer. Three orange dotted line parts are used to calculate precision, convergence rate, and classification accuracy.  $|X\rangle$  and  $|Z\rangle$  are the quantum states of training data before and after QRDR. Similarly,  $|q\rangle$  and  $|z_q\rangle$  correspond to the data to be classified.  $y_q$  is the predicted label of  $y$ .

TABLE I. Comparison of the complexity of several different quantum dimensionality reduction algorithms with QRDR.

	Time complexity	Space complexity
QRDR	$O(d, \text{polylog}(MN)/\epsilon)$	$O(\log R + \log(MN))$
QPE-DR [12, 13]	$O(d, \text{polylog}(MN)/\epsilon^3)$	$O(\log 1/\epsilon + \log R + \log(MN))$
QPCA [9, 24]	$O(M \text{polylog}(MN)/\epsilon^3)$	$O(\log(MN))$

sample,  $y_i$ , can be determined by calculating the inner product of the state  $|\eta_0, \eta\rangle$  with the new sample state. This paper primarily focuses on dimensionality reduction, so the QSVM component is not covered in detail. For more comprehensive information, please refer to prior literature [27, 35, 36].

This dataset contains  $M = 208$  samples, each with  $N = 60$  features. First, the unitary operator  $e^{-i\mathcal{H}t}$  is directly applied to the states. The input state is

$$|\Psi_{in}\rangle = \sum_{k=1}^M \sum_{j=1}^N x_k^j |j\rangle |k\rangle. \quad (27)$$

We set  $R = 16$  and varied  $c$  proportionately from 0.001 to 0.032. After applying QRDR to the input data, the simulation error is shown in Fig. 2. The error defined in Eq. 21 represents the deviation between the numerical simulation results of QRDR and the theoretical results of the classical DR.

Simulation results indicate that the discrepancy between the QRDR output and theoretical expectations aligns with the theoretical predictions based on the parameter  $c$ . By calculating the linear fitting coefficients of  $\log(1/c)$  and  $\log(1/\epsilon^{0.5})$ , we can evaluate whether the two parameters are linearly correlated. For  $R = 16$ , the correlation coefficient is 0.9835, while for  $R = 8$ , it is 0.9948. This strong linear correlation between  $c$  and  $\epsilon^{0.5}$  confirms the accuracy of our theoretical analysis. Next, we use the quantum data processed by QRDR and the original

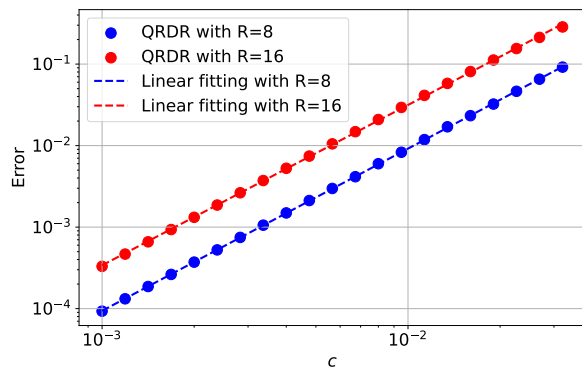


FIG. 3. The error of QRDR with different  $c$ . Red points are simulating results of QSVM in classical computer in  $R = 16$  and blue line is in  $R = 8$ . The dashed line is the result of a linear fit of error and  $c$ .

quantum data as different input sets for the QSVM. By comparing the training results and complexity of QSVM, we can evaluate the performance of QRDR.

The data is divided into 8 groups, each containing 26 samples, following the standard K-fold cross-validation procedure. Seven sets of data are used as the training set, while one set serves as the test set. Eight QSVM models are trained, and the average accuracy across these models is taken as the final accuracy. For the original data with

$N = 60$  features, the accuracy is 0.8625. For  $R = 16$ , the accuracy improves to 0.8937.

Next, we select 20 random samples as the validation set and use the remaining data to train the parameters, repeating the process eight times to assess the performance of QSVM with different reduced dimensions  $R$  of input data. We observe that QSVM performs very well with  $R = 8$ . When using higher dimensions like  $R = 16$  and  $R = 32$ , there is only a marginal increase in accuracy. This suggests that only around 8 parameters are necessary to capture the features of the samples in this dataset. The accuracy of QSVM is illustrated in Fig. 4.

The complexity of QSVM is  $O(\log MN)$ , where  $N$  is the dimensionality and  $M$  is the number of samples [8, 37]. If the dimensionality after QRDR is set to  $R = O(\log N)$ , the complexity of QSVM with QRDR becomes  $O(\log M \log N)$ , providing a speedup at this stage.

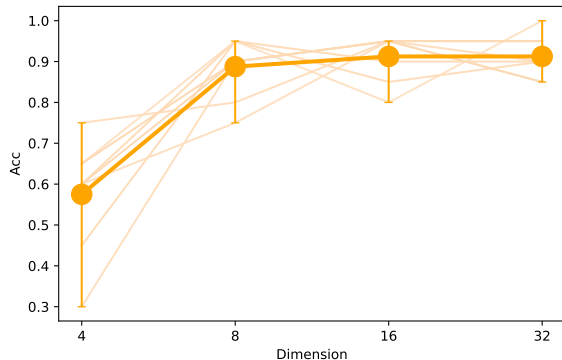


FIG. 4. The accuracy of QSVM is presented with varying input data dimensions  $R$ . The dots represent the average accuracy across multiple calculations, while the upper and lower bounds of the error bars represent the maximum and minimum accuracies observed across multiple calculations. Apart from  $R = 4$ , QSVM is effective at classifying the data

By simulating the QRDR and QSVM, the error rate of QRDR aligns with our expectations, while the accuracy of QSVM improves and complexity decreases. Our QRDR algorithm enhances the accuracy and speed of QSVM classification, demonstrating its practical value. More details about QSVM, including its workflow and parameter optimization process, can be found in prior work [8, 35].

## B. QRDR FOR QUANTUM MANY BODY PHASE CLASSIFICATION

In this section, the quantum phase classification of 1D Transverse-field Ising model(TFIM) is performed to verify the practicability of our QRDR algorithm.

1D TFIM is a fundamental toy model for quantum phase transition, which consider the nearest neighbor  $ZZ$  interaction as well as an extra x-direction transverse mag-

netic field in a spin-half chain, with hamiltonian

$$H = -J \sum_{i,i+1} \sigma_i^z \sigma_{i+1}^z + h \sum_i \sigma_i^x. \quad (28)$$

This Hamiltonian is invariant under a global  $Z_2$  transformation,  $\tau = \prod_i \sigma_x$ . Because of the competition of the two non-commute parts in Eq.(28), quantum phase transition appears at the critical point  $h/J = 1$ . In the region  $h > J$ , there is a unique ground state that preserve the  $Z_2$  symmetry and this system is in a disordered paramagnetic phase. In the region  $h < J$ ,  $Z_2$  symmetry is spontaneously broken in the thermodynamic limit, this system is in an ordered ferromagnetic phase.

We first use QRDR to reduce the dimension of quantum state, and then use a QCNN model based on Ref. [38] to classify the quantum state before and after QRDR respectively. In this case, we simulate a complete quantum convolutional neural network model, including a dimension reduction layer, a convolutional layer, a pooling layer, and a full-connected layer, as shown in Fig. III B.

Operator  $S$  is the ansatz to generate superposition state in the ancillary system. The ansatz[39] we used for the four ancillary qubits contains 28 trainable parameters, and is shown in Fig. 6(a). For the convolutional layer, the nine operators  $Q_0, Q_1, \dots, Q_8$  consist of the convolution operator.  $Q_k$  is the tensor product of two of the following three operators,  $E_1, E_2$  and  $E_3$ .  $E_2$  is the identity matrix and  $E_3 = E_1^\dagger$ , where

$$E_1(i, j) = \begin{cases} 1 & (i = j + 1), (i = 0, j = 2^r) \\ 0 & Else. \end{cases} \quad (29)$$

We primarily need to provide the decomposition method for  $E_1$ .  $E_1$  can be constructed using a combination of  $O(r^3)$  CNOT gates and Pauli  $X$  gates, as illustrated in Fig. 6(b).

The function of pooling layer after the convolutional layer is to reduce the spatial size so as to reduce the amount of parameters. Here we choose  $R_y(\theta = 0)$ . The entire QCNN network consists of 3 layers with a total of 84 trainable parameterized quantum gates. The loss function is related to the expectation value of the parameterized Hamiltonian  $e(p) = \langle p | \mathcal{H} | p \rangle$ . This Hamiltonian consists of identity operators  $I$  and Pauli operators  $\sigma_z$ ,

$$\mathcal{H} = h^0 I + \sum_i h^i \sigma_z^i + \sum_{i,j} h^{ij} \sigma_z^i \sigma_z^j \quad (30)$$

where  $h^0, h^i, h^{ij}$  are the parameters, and Roman indices  $i, j$  denote location of the qubit. On the other hand, the classical neural network is composed of three fully connected layers, each containing 128 neurons. In both models, we randomly divided a total of 200 data points into 160 training data and 40 testing data. The training set utilized a batch size of 20, and the training process was performed for 20 epochs. The optimizer used was

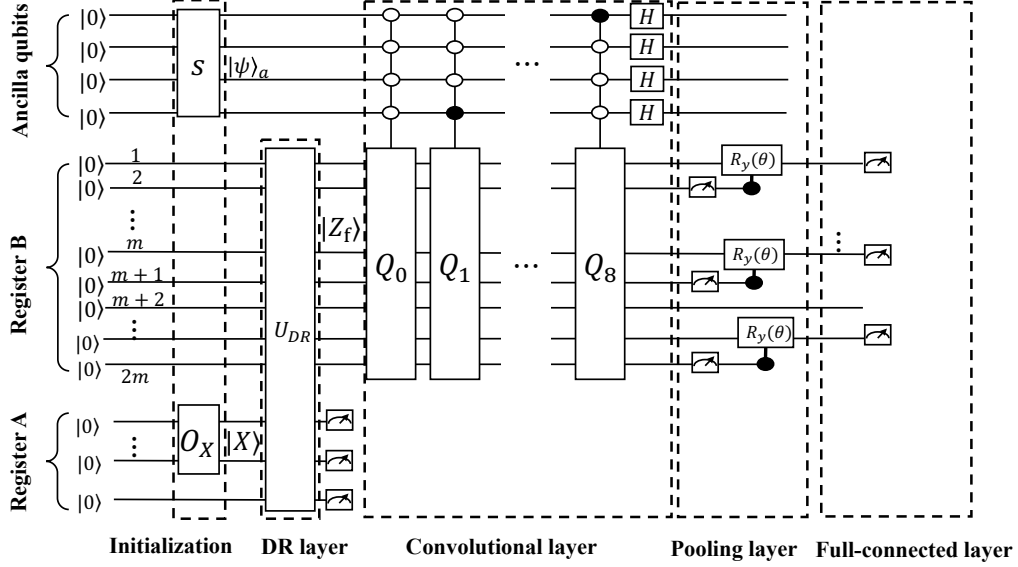


FIG. 5. The simplified quantum circuit of QRDR-QCNN algorithm. The initial state  $|X\rangle$  is prepared in register A by operator  $O_X$ , and QRDR utilizes a probe qubit and state  $|X\rangle$  to prepare state  $|Z\rangle$  after DR in register B. Then, QCNN employs ancillary qubits to process state  $|Z\rangle$  with the linear combination of unitary operators  $Q_0, Q_1, \dots, Q_8$  which can act as a group of convolution operator.

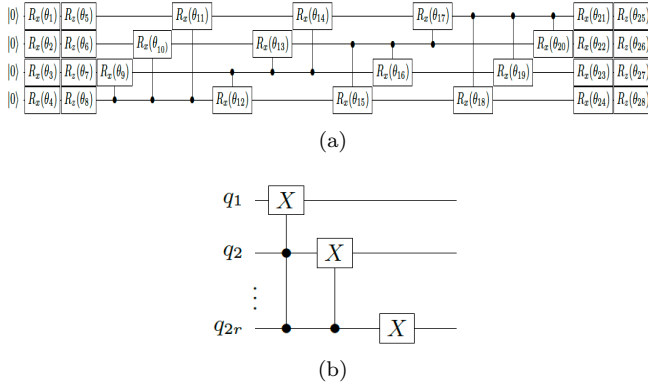


FIG. 6. (a) Quantum circuit for realizing operator  $S$ . (b) Decomposition of operator  $E_1$  in the form of basic gates.

Adam, and the loss function employed was the cross-entropy loss function. The numerical simulation is carried out on 'MindSore Quantum' platform and the results indicate that QRDR can improve both the performance of QCNN and CNN. Moreover, QCNN with QRDR can extremely reduce the training parameter and computation complexity, achieving higher accuracy. The simulation results are shown in Fig. 7.

The Hamiltonian in Eq. (28) can be directly linked to a p-wave superconducting Hamiltonian via the Jordan-Wigner transformation. In this context, two dangling Majorana fermions can be found at the end of the chain under open boundary conditions. This implies that our QRDR method can be used to distinguish between dif-

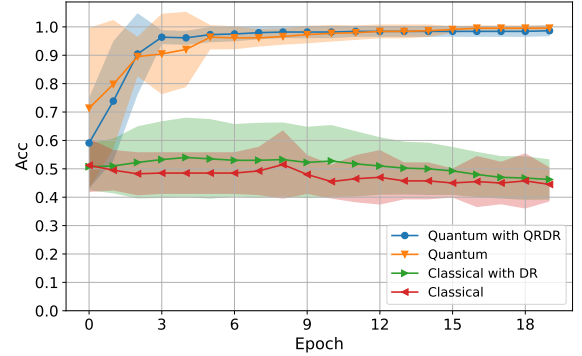


FIG. 7. The performance of QRDR plus QCNN. The blue, orange, green, and red curves denote the average accuracy of the QCNN with QRDR, QCNN, CNN with DR, and CNN, respectively. The shadow areas of the corresponding color denote the accuracy fluctuation range in the 10 times simulation results.

ferent symmetry-protected topological phases as well as genuine topological phases. Topological states, which are independent of local perturbations, have fewer dominant components in the state vector, allowing for natural compression of the state.

#### IV. DISCUSSION

To summarize, we propose a novel quantum dimension reduction algorithm called QRDR for preprocessing high-dimensional quantum data prior to the application of quantum machine learning algorithms. In comparison to existing quantum DR algorithms, such as QPE-based algorithms and VQA-based algorithms, it offers distinct advantages in terms of computational complexity and qubit resources by employing QRT. We employ QRDR alongside two different quantum machine learning models, QSVM and QCNN, to evaluate our algorithm's efficacy. Our method effectively accomplishes two critical tasks: classifying underwater detection targets and analyzing quantum many-body phases. The simulation results demonstrate its effective reduction of dimensionality in quantum data, thereby enhancing the performance and speed of subsequent algorithms. Given these aforementioned advantages, QRDR is poised to play a significant role in the future era of general quantum computing. Despite our reduction in quantum resource consumption, achieving large-scale algorithm demonstrations on NISQ

devices still presents many challenges.

#### V. ACKNOWLEDGEMENTS.

S.W. acknowledges the National Natural Science Foundation of China under Grants No. 12005015 and Beijing Nova Program under Grants No. 20230484345; We acknowledge the National Key Research and Development Program of China (2017YFA0303700); Beijing Advanced Innovation Center for Future Chip (ICFC). P. G. acknowledges the National Natural Science Foundation of China under grant No. 12247164. T.X acknowledges the the National Natural Science Foundation of China No.12275117, Guangdong Basic and Applied Basic Research Foundation No.2022B1515020074.

#### VI. DATA AVAILABILITY STATEMENT

The data that support the findings of this study are available on [40].

- 
- [1] John W. Goodell, Satish Kumar, Weng Marc Lim, and Debidutta Pattnaik. Artificial intelligence and machine learning in finance: Identifying foundations, themes, and research clusters from bibliometric analysis. *Journal of Behavioral and Experimental Finance*, 32:100577, 2021. ISSN 2214-6350. URL <https://www.sciencedirect.com/science/article/pii/S2214635021001210>.
- [2] Hamed Ghoddusi, Germán G. Creamer, and Nima Rafizadeh. Machine learning in energy economics and finance: A review. *Energy Economics*, 81:709–727, 2019. ISSN 0140-9883. URL <https://www.sciencedirect.com/science/article/pii/S0140988319301513>.
- [3] Bradley J. Erickson, Panagiotis Korfiatis, Zeynetin Akkus, and Timothy L. Kline. Machine learning for medical imaging. *RadioGraphics*, 37(2):505–515, 2017. URL <https://doi.org/10.1148/rg.2017160130>. PMID: 28212054.
- [4] Rahul C. Deo. Machine learning in medicine. *Circulation*, 132(20):1920–1930, 2015. URL <https://www.ahajournals.org/doi/abs/10.1161/CIRCULATIONAHA.115.001593>.
- [5] Yaswitha Gujju, Atsushi Matsuo, and Rudy Raymond. Quantum machine learning on near-term quantum devices: Current state of supervised and unsupervised techniques for real-world applications, 2023. URL <https://arxiv.org/abs/2307.00908>.
- [6] Vedran Dunjko and Hans J Briegel. Machine learning and artificial intelligence in the quantum domain: a review of recent progress. *Reports on Progress in Physics*, 81(7): 074001, jun 2018. URL <https://dx.doi.org/10.1088/1361-6633/aab406>.
- [7] Iordanis Kerenidis and Anupam Prakash. Quantum recommendation systems. *arXiv preprint arXiv:1603.08675*, 2016. URL <https://arxiv.org/pdf/1603.08675>.
- [8] Patrick Rebentrost, Masoud Mohseni, and Seth Lloyd. Quantum support vector machine for big data classification. *Physical Review Letters*, 113:130503, Sep 2014. URL <https://link.aps.org/doi/10.1103/PhysRevLett.113.130503>.
- [9] Seth Lloyd, Masoud Mohseni, and Patrick Rebentrost. Quantum principal component analysis. *Nature Physics*, 10(9):631–633, 2014. URL <https://www.nature.com/articles/nphys3029>.
- [10] Amira Abbas, David Sutter, Christa Zoufal, Aurélien Lucchi, Alessio Figalli, and Stefan Woerner. The power of quantum neural networks. *Nature Computational Science*, 1(6):403–409, 2021. URL <https://doi.org/10.1038/s43588-021-00084-1>.
- [11] Kerstin Beer, Dmytro Bondarenko, Terry Farrelly, Tobias J Osborne, Robert Salzmänn, Daniel Scheiermann, and Ramona Wolf. Training deep quantum neural networks. *Nature communications*, 11(1): 808, 2020. URL <https://www.nature.com/articles/s41467-020-14454-2>.
- [12] YaoChong Li, Ri-Gui Zhou, RuiQing Xu, WenWen Hu, and Ping Fan. Quantum algorithm for the nonlinear dimensionality reduction with arbitrary kernel. *Quantum Science and Technology*, 6(1):014001, nov 2020. URL <https://dx.doi.org/10.1088/2058-9565/abbe66>.
- [13] Chao-Hua Yu, Fei Gao, Song Lin, and Jingbo Wang. Quantum data compression by principal component analysis. *Quantum information processing*, 18(8), 1 2019. URL <https://doi.org/10.1007/s11128-019-2364-9>.
- [14] Jin-Min Liang, Shu-Qian Shen, Ming Li, and Lei Li. Variational quantum algorithms for dimensionality reduction and classification. *Physical Review A*, 101:032323, Mar 2020. URL <https://link.aps.org/doi/10.1103/PhysRevA.101.032323>.

- [15] Jonathan Romero, Jonathan P Olson, and Alan Aspuru-Guzik. Quantum autoencoders for efficient compression of quantum data. *Quantum Science and Technology*, 2(4): 045001, aug 2017. URL <https://dx.doi.org/10.1088/2058-9565/aa8072>.
- [16] Chang-Jiang Huang, Hailan Ma, Qi Yin, Jun-Feng Tang, Daoyi Dong, Chunlin Chen, Guo-Yong Xiang, Chuan-Feng Li, and Guang-Can Guo. Realization of a quantum autoencoder for lossless compression of quantum data. *Physical Review A*, 102:032412, Sep 2020. URL <https://link.aps.org/doi/10.1103/PhysRevA.102.032412>.
- [17] Bojia Duan, Jiabin Yuan, Juan Xu, and Dan Li. Quantum algorithm and quantum circuit for a-optimal projection: Dimensionality reduction. *Physical Review A*, 99: 032311, Mar 2019. URL <https://link.aps.org/doi/10.1103/PhysRevA.99.032311>.
- [18] Shi-Jie Pan, Lin-Chun Wan, Hai-Ling Liu, Qing-Le Wang, Su-Juan Qin, Qiao-Yan Wen, and Fei Gao. Improved quantum algorithm for a-optimal projection. *Physical Review A*, 102:052402, Nov 2020. URL <https://link.aps.org/doi/10.1103/PhysRevA.102.052402>.
- [19] Kai Yu, Song Lin, and Gong-De Guo. Quantum dimensionality reduction by linear discriminant analysis. *Physica A: Statistical Mechanics and its Applications*, 614:128554, 2023. ISSN 0378-4371. URL <https://www.sciencedirect.com/science/article/pii/S0378437123001097>.
- [20] Iris Cong and Luming Duan. Quantum discriminant analysis for dimensionality reduction and classification. *New Journal of Physics*, 18(7):073011, jul 2016. URL <https://dx.doi.org/10.1088/1367-2630/18/7/073011>.
- [21] Xi He, Li Sun, Chufan Lyu, and Xiaoting Wang. Quantum locally linear embedding for nonlinear dimensionality reduction. *Quantum Information Processing*, 19:1–21, 2020. URL <https://doi.org/10.1007/s11128-020-02818-y>.
- [22] Gagan Sidhu. Locally linear embedding and fmri feature selection in psychiatric classification. *IEEE Journal of Translational Engineering in Health and Medicine*, 7:1–11, 2019. URL <https://ieeexplore.ieee.org/document/8807145>.
- [23] Zhaokai Li, Xiaomei Liu, Hefeng Wang, Sahel Ashhab, Jiangyu Cui, Hongwei Chen, Xinhua Peng, and Jiangfeng Du. Quantum simulation of resonant transitions for solving the eigenproblem of an effective water hamiltonian. *Physical Review Letters*, 122:090504, Mar 2019. URL <https://link.aps.org/doi/10.1103/PhysRevLett.122.090504>.
- [24] Zhaokai Li, Zihua Chai, Yuhang Guo, Wentao Ji, Mengqi Wang, Fazhan Shi, Ya Wang, Seth Lloyd, and Jiangfeng Du. Resonant quantum principal component analysis. *Science Advances*, 7(34):eabg2589, 2021. URL <https://www.science.org/doi/abs/10.1126/sciadv.abg2589>.
- [25] Vittorio Giovannetti, Seth Lloyd, and Lorenzo Maccone. Quantum random access memory. *Physical Review Letters*, 100:160501, Apr 2008. URL <https://link.aps.org/doi/10.1103/PhysRevLett.100.160501>.
- [26] Hefeng Wang. Quantum algorithm for obtaining the eigenstates of a physical system. *Physical Review A*, 93: 052334, May 2016. URL <https://link.aps.org/doi/10.1103/PhysRevA.93.052334>.
- [27] Fan Yang, Xinyu Chen, Dafa Zhao, Shijie Wei, Jingwei Wen, Hefeng Wang, Tao Xin, and Guilu Long. Quantum multi-round resonant transition algorithm. *Entropy*, 25 (1), 2023. ISSN 1099-4300. URL <https://www.mdpi.com/1099-4300/25/1/61>.
- [28] Guang Hao Low and Isaac L. Chuang. Optimal hamiltonian simulation by quantum signal processing. *Physical Review Letters*, 118:010501, Jan 2017. URL <https://link.aps.org/doi/10.1103/PhysRevLett.118.010501>.
- [29] Xiao Yuan, Suguru Endo, Qi Zhao, Ying Li, and Simon C Benjamin. Theory of variational quantum simulation. *Quantum*, 3:191, 2019. URL <https://quantum-journal.org/papers/q-2019-10-07-191/>.
- [30] Cristina Cirstoiu, Zoe Holmes, Joseph Iosue, Lukasz Cincio, Patrick J Coles, and Andrew Sornborger. Variational fast forwarding for quantum simulation beyond the coherence time. *Npj Quantum Information*, 6(1): 1–10, 2020. URL <https://www.nature.com/articles/s41534-020-00302-0>.
- [31] Ying Li and Simon C. Benjamin. Efficient variational quantum simulator incorporating active error minimization. *Physical Review X*, 7:021050, Jun 2017. URL <https://link.aps.org/doi/10.1103/PhysRevX.7.021050>.
- [32] Aram W. Harrow, Avinandan Hassidim, and Seth Lloyd. Quantum algorithm for linear systems of equations. *Physical Review Letters*, 103:150502, Oct 2009. URL <https://link.aps.org/doi/10.1103/PhysRevLett.103.150502>.
- [33] Hrushikesh Patil, Yulun Wang, and Predrag S. Krstić. Variational quantum linear solver with a dynamic ansatz. *Physical Review A*, 105:012423, Jan 2022. URL <https://link.aps.org/doi/10.1103/PhysRevA.105.012423>.
- [34] Hsin-Yuan Huang, Kishor Bharti, and Patrick Rebentrost. Near-term quantum algorithms for linear systems of equations, 2019. URL <https://arxiv.org/abs/1909.07344>.
- [35] Fan Yang, Dafa Zhao, Chao Wei, Xinyu Chen, Shijie Wei, Hefeng Wang, Guilu Long, and Tao Xin. A parallel quantum eigensolver for quantum machine learning. *New Journal of Physics*, 26(4):043011, apr 2024. URL <https://dx.doi.org/10.1088/1367-2630/ad15b4>.
- [36] Feng Xu, Fan Yang, Chao Wei, Xinyu Chen, Shijie Wei, Hefeng Wang, Jun Li, and Tao Xin. Quantum simulation of water-molecule bond angles using an nmr quantum computer. *Physical Review A*, 109:042618, Apr 2024. URL <https://link.aps.org/doi/10.1103/PhysRevA.109.042618>.
- [37] Zhaokai Li, Xiaomei Liu, Nanyang Xu, and Jiangfeng Du. Experimental realization of a quantum support vector machine. *Physical Review Letters*, 114:140504, Apr 2015. URL <https://link.aps.org/doi/10.1103/PhysRevLett.114.140504>.
- [38] ShiJie Wei, YanHu Chen, ZengRong Zhou, and GuiLu Long. A quantum convolutional neural network on nisq devices. *AAPPS Bulletin*, 32:1–11, 2022. URL <https://doi.org/10.1007/s43673-021-00030-3>.
- [39] Sukin Sim, Peter D Johnson, and Alán Aspuru-Guzik. Expressibility and entangling capability of parameterized quantum circuits for hybrid quantum-classical algorithms. *Advanced Quantum Technologies*, 2(12):1900070, 2019. URL <https://doi.org/10.1002/qute.201900070>.
- [40] MindQuantum Developer. Mindquantum, version 0.6.0, March 2021. URL [https://gitee.com/mindspore/mindquantum/tree/research/paper\\_with\\_code/quantum\\_resonant\\_dimensionality\\_reduction\\_and\\_](https://gitee.com/mindspore/mindquantum/tree/research/paper_with_code/quantum_resonant_dimensionality_reduction_and_)

`application_in_quantum_machine_learning.`